*The following article appeared in (**J. Chem. Phys.**, **145**, 211905, **2016**) and may be found at (http://dx.doi.org/10.1063/1.4959846).*

A cavitation transition in the energy landscape of simple cohesive liquids and glasses

Y. Elia Altabet, Frank H. Stillinger, and Pablo G. Debenedetti

Citation: The Journal of Chemical Physics **145**, 211905 (2016); doi: 10.1063/1.4959846
View online: http://dx.doi.org/10.1063/1.4959846
View Table of Contents: http://aip.scitation.org/toc/jcp/145/21
Published by the American Institute of Physics

THE JOURNAL OF CHEMICAL PHYSICS **145**, 211905 (2016)

A cavitation transition in the energy landscape of simple cohesive liquids and glasses

Y. Elia Altabet,[1] Frank H. Stillinger,[2] and Pablo G. Debenedetti[1,a)]
[1]*Department of Chemical and Biological Engineering, Princeton University, Princeton, New Jersey 08544, USA*
[2]*Department of Chemistry, Princeton University, Princeton, New Jersey 08544, USA*

(Received 16 May 2016; accepted 14 July 2016; published online 28 July 2016)

In particle systems with cohesive interactions, the pressure-density relationship of the mechanically stable inherent structures sampled along a liquid isotherm (i.e., the equation of state of an energy landscape) will display a minimum at the Sastry density ρ_S. The tensile limit at ρ_S is due to cavitation that occurs upon energy minimization, and previous characterizations of this behavior suggested that ρ_S is a spinodal-like limit that separates all homogeneous and fractured inherent structures. Here, we revisit the phenomenology of Sastry behavior and find that it is subject to considerable finite-size effects, and the development of the inherent structure equation of state with system size is consistent with the finite-size rounding of an athermal phase transition. What appears to be a continuous spinodal-like point at finite system sizes becomes discontinuous in the thermodynamic limit, indicating behavior akin to a phase transition. We also study cavitation in glassy packings subjected to athermal expansion. Many individual expansion trajectories averaged together produce a smooth equation of state, which we find also exhibits features of finite-size rounding, and the examples studied in this work give rise to a larger limiting tension than for the corresponding landscape equation of state. *Published by AIP Publishing.* [http://dx.doi.org/10.1063/1.4959846]

I. INTRODUCTION

The macroscopic physics observed in an experiment or molecular simulation is encoded in the microscopic interactions among constituent species. In turn, such interactions, often approximated in simulations as a pairwise potential, must contain a minimal set of "ingredients" to give rise to particular phenomena. Obtaining a comprehensive understanding of the macroscopic consequences of such interactions both enriches our scientific understanding of the natural world and provides a basis for the rational design of engineered systems with tailored interactions.

In the context of fluid phase behavior, one feature of the intermolecular pair potential that has received much attention is the attractive interaction among constituents. While the physics of dense simple liquids is largely governed by short-range repulsive interactions,[1,2] thermodynamically distinct vapor and liquid phases do not exist without attractive interactions. In other words, a dense "liquid" with no attractive interactions, when undergoing continuous decompression, will form a "vapor" without cavitation. Even with attractive interactions, the range of such interactions will dictate if the vapor/liquid binodal exists in a stable region of the phase diagram,[3–5] a fact that has implications in the crystallization of proteins.[6] A number of works have considered how the existence and range of attractive interactions affect the structure and dynamics of thermal fluid systems.[7–13]

The present work explores features of the energy landscape in several systems that have sufficient cohesive interactions to exhibit a vapor/liquid transition. Specifically, we will consider the equation of state of their energy landscape,[14,15] that is to say the pressure-density relationship of the inherent structures generated along a liquid isotherm. The inherent structure formalism[16,17] allows one to decouple structural and thermal contributions to a system's behavior. In any configuration, a liquid will find itself within a given basin of attraction that is uniquely associated with one of the many local minima on its high-dimensional potential energy hypersurface. Characterizing the mechanically stable packings (i.e., inherent structures) that are produced through mapping a given configuration to its local potential energy minimum has provided physical insights into numerous topics in condensed matter physics, most notably in the context of supercooled liquids and the glass transition.[18–22]

The nature of the inherent structures produced from systems with and without attractive interactions appears to reflect the presence or absence of a distinct vapor/liquid phase transition. Specifically, there exist qualitative differences between the equations of state of their energy landscape. A schematic illustrating the difference between the equations of state of a system of particles interacting through a purely repulsive, finite-ranged potential (e.g., Weeks-Chandler-Andersen) and one with an attractive tail (e.g., Lennard-Jones) is shown in Figure 1.

For systems composed of particles with purely repulsive interactions that decay to zero at finite distance (e.g., Hookean, Hertzian, and Weeks-Chandler-Andersen interactions), the equation of state of the energy landscape is akin to curve (i) in Fig. 1. A salient feature of this curve is that at low enough density, the pressure reaches zero and remains so upon any further decompression of the parent fluid. In this

a)Author to whom correspondence should be addressed. Electronic mail: pdebene@princeton.edu

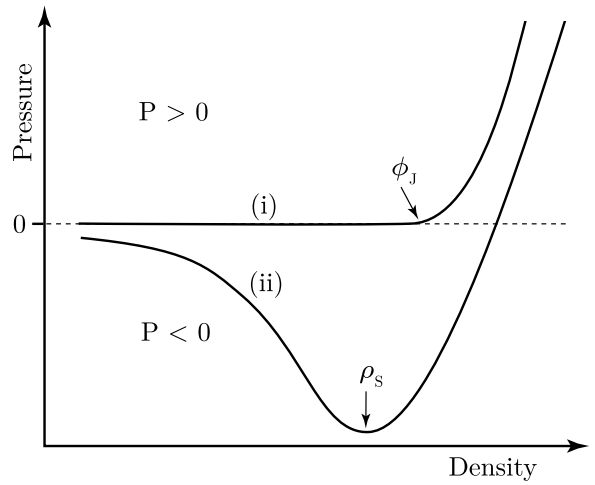

FIG. 1. Schematic representation of the equation of state of the energy landscape of a system of particles interacting through a purely repulsive, finite-ranged pair potential (i) and a potential with attractive interactions (ii). Curve (i) will reach zero pressure and remain so at densities lower than the jamming threshold ϕ_J. Curve (ii) can extend to negative pressure due to cohesive interactions and reaches a mechanical instability at the Sastry density ρ_S where further decompression of the parent liquid results in lower tension in the underlying inherent structures.

region, the inherent structures can reach their global potential energy minimum, namely zero, as all particles can distance themselves from each other beyond the range of interaction. The region where the pressure crosses between positive and zero in such systems is often called point J (density ϕ_J), and characterizing the behavior of inherent structures in the neighborhood of ϕ_J has received much attention in the context of the jamming scenario.[23–26] In addition, such studies often employ sequential volume expansion and energy minimization (athermal quasistatic expansion) as a method of probing the behavior of packings as they approach this crossover.[25,27] The latter method is convenient as any expansion run will have a well-defined point where the pressure becomes zero, while quenching from an equilibrium fluid in the neighborhood of ϕ_J will yield a distribution of jammed and un-jammed packings.[25]

For model systems with attractive interactions typical of real molecular liquids, much of the intellectual framework (that we will ultimately build upon here) has been developed by Sastry and co-workers.[28–30] However, the first report of the phenomenology discussed here is credited to LaViolette.[31] For systems with attractive interactions such as pure component[29,31] and binary[30,32] Lennard-Jones, *ortho*-terphenyl,[33] alkanes,[34,35] molten zinc(II) bromide,[36] and SPC/E water,[15] the inherent structures generated along a liquid isotherm have an equation of state similar to curve (ii) in Figure 1. At low enough density the inherent structure equation of state extends to negative pressure, as the cohesive interactions among particles allow the system to support isotropic tension. The inherent structures continue to withstand greater tension upon decompression of the parent liquid until reaching a minimum at ρ_S, the Sastry density. Below ρ_S, the inherent structures are unable to sustain further tension.

The physical process associated with the tensile limit occurring at ρ_S is the yielding of the inherent structures, in other words their mechanical failure. An example of an inherent structure produced slightly below ρ_S in a binary mixture is presented in the left-hand side of Fig. 2. The yielding below ρ_S is associated with formation of compact voids that emerge upon energy minimization. An instantaneous interface[37] rendering of the cavity is shown in Fig. 2 on the right. This void appears similar to critical nuclei reported in studies of homogeneous bubble nucleation (e.g., see Figure 4 of Ref. 38). Liquids subject to isothermal decompression will sample fractured inherent structures at densities well above the binodal if the temperature is sufficiently high. In other words, cavitation in the thermal liquid and cavitation in its inherent structures can be well-separated phenomena. It should be noted, however, that we have found this cavitation of inherent structures is preserved for fluids sampled along supercritical isotherms.

Due to the shape of the inherent structure equation of state resembling a mean field liquid isotherm as well as the physical process representing a mechanical failure, the Sastry point was interpreted as a singular spinodal-like point for a liquid's inherent structures. Above ρ_S all inherent structures are homogeneous, and below ρ_S all are broken. It was suggested that the Sastry point represented the $T = 0$ limit of the liquid spinodal as well as the limit of stability for the homogeneous glassy state.[14,29,39] Mean-field calculations supported the notion that the liquid spinodal and the Kauzmann locus (collection of state points corresponding to equal entropy between liquid and crystal) intersect at zero temperature.[14] Later work suggests that the liquid spinodal and glass transition line do intersect at ρ_S, however, they do so at finite temperature.[30,33,40]

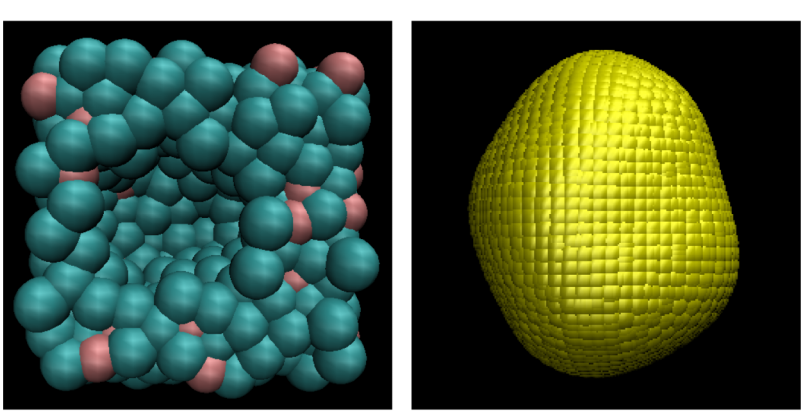

FIG. 2. Energy minimization of a liquid configuration below the Sastry density for an 80:20 binary mixture of 500 particles interacting via a (7,6) generalized Lennard-Jones potential (see Sec. II for details on the potential). The image on the left presents an example of an inherent structure that has fractured upon minimization to create an internal cavity (cyan = A particles; pink = B particles). On the right is an instantaneous interface representation of the void space produced in the same configuration.

In this paper, we revisit the phenomenology of Sastry behavior with interactions typical of simple molecular liquids. In particular, we consider the behavior of two binary mixtures whose interactions are part of the (n,6) generalized Lennard-Jones potential (described in Sec. II). In Section III, we consider a system with an inherent structure equation of state similar to curve (ii) in Fig. 1 and show that in the region below ρ_S, the liquid samples a mix of fractured (low tension) and homogenous (high tension) inherent structures, resulting in a bimodal distribution of inherent structure properties. A portion of the equation of state below ρ_S represents an average between distinct low and high tension branches. Thus, the Sastry density in such a system appears to signify the *onset* of fracture rather than being singular in nature. Next, in Section IV, we show that the observed bimodality and the inherent structure equation of state are subject to considerable finite size effects. The behavior of the inherent structure equation of state as system size increases is similar to the finite-size rounding of the first order vapor/liquid transition, suggesting that the Sastry point represents an athermal phase transition. This section also contains a characterization of the void space as well as a discussion of the role of potential softening in the context of Sastry behavior. Section V includes a discussion of behavior in the thermodynamic (infinite system) limit, where we suggest that in this limit, the inherent structure pressure P_{IS} becomes discontinuous at ρ_S as the parent liquid jumps abruptly from sampling homogeneous (high tension) to fractured (low tension) inherent structures. In Section VI, we present results of athermal quasistatic expansion and show that the physics is qualitatively (but not quantitatively) similar to quenching from an equilibrium liquid. Qualitative differences do arise at low density between quenches of a supercritical fluid and athermal expansion. Section VII contains concluding remarks as well as suggestions for further study.

II. METHODS

A. Interaction potential

In this work we employ a recently introduced[41] generalized (n,6) Lennard-Jones pair potential

$$\phi(r) = 4\epsilon\left[\lambda\left(\frac{\sigma}{r}\right)^n - \alpha\left(\frac{\sigma}{r}\right)^6\right]. \tag{1}$$

The coefficients λ and α are defined as

$$\lambda = \frac{3}{2}\left(\frac{2^{n/6}}{n-6}\right), \quad \alpha = \frac{n}{2(n-6)}, \tag{2}$$

and are designed such that, upon varying n, the location of the minimum and the well depth are unchanged with respect to the values for the standard (12,6) Lennard-Jones potential. One feature of this (n,6) family is that it allows one to continuously tune potential softness. In this study, we focus on the (12,6) and (7,6) variants of the potential. The attractive well of the softer (7,6) version is wider than the more typical (12,6) version. Here, we employ a cut-off $r_c = 3.5$ with force shifting of the potential to ensure that both the potential and the force between two particles are zero at the cut-off and beyond,

$$\phi^{fs}(r) = \begin{Bmatrix} \phi(r) - \phi(r_c) - (r - r_c)\,\phi'(r_c) & r \le r_c \\ 0 & r > r_c \end{Bmatrix}. \tag{3}$$

B. Simulation details

In this work, we study a binary 80:20 mixture with the frequently employed Kob-Andersen[42] parameters: $\epsilon_{AA} = 1.0$, $\sigma_{AA} = 1.0$; $\epsilon_{AB} = 1.5$, $\sigma_{AB} = 0.8$; $\epsilon_{BB} = 0.5$, $\sigma_{BB} = 0.88$. This model is closely related to the one employed in earlier studies of amorphous $Ni_{80}P_{20}$.[43,44] All masses are the same, and we report results in the traditional reduced units in terms of the AA interaction parameters.

Molecular dynamics is performed in a cubic simulation box with periodic boundary conditions in the NVT ensemble. Time integration is performed via the velocity Verlet algorithm with a molecular dynamics time step of 0.002 in the LAMMPS[45] software package. Simulations performed at fixed temperature employ a Nosé-Hoover thermostat.[46] Inherent structures are generated through energy minimization at fixed density using the Polak and Ribiere[47] method of conjugate gradients. Minimization was considered complete if the relative change in energy per iteration was less than 10^{-8}. All images of simulation configurations are rendered in VMD.[48]

III. THE SASTRY DENSITY AS AN ONSET POINT

Earlier presentations of the equation of state of an energy landscape[14] divided the equation of state into three density intervals: (I) densities where pressure is positive, (II) densities characterized by negative pressure and positive slope, and (III) densities below the minimum where the slope is negative. The minimum that separates regions II and III is called the Sastry point, which is defined by its density ρ_S and the corresponding pressure P_S. In this section, we will provide an example of a system that has an inherent structure equation of state akin to previous observations. However, additional analysis shows that the Sastry point in this system represents the *onset* of fracture rather than an abrupt transition from homogeneous to broken.

In Figure 3, we present the equation of state of the energy landscape for the (7,6) version of the potential for a system size of 500 particles sampled along the $T = 1.0$ liquid isotherm. In agreement with previous observations,[30] this equation of state is fairly insensitive to the liquid's temperature as long as cavitation in the liquid is avoided. In Fig. 3, vertical solid lines define the three regimes of this equation of state discussed above. As density is reduced from $\rho = 1.50$, the average inherent structure pressure is positive and decreases monotonically, reaching zero at roughly $\rho = 1.41$. Densities below 1.41 result in inherent structures under isotropic tension, a feature that is only possible due to the attractive interactions in the pair potential. Reducing density further results in greater tension until a minimum occurs at $\rho_S = 1.188$ and $P_S = -6.338$, the Sastry point for this system. Below the Sastry density, reduction in density results in a reduction of

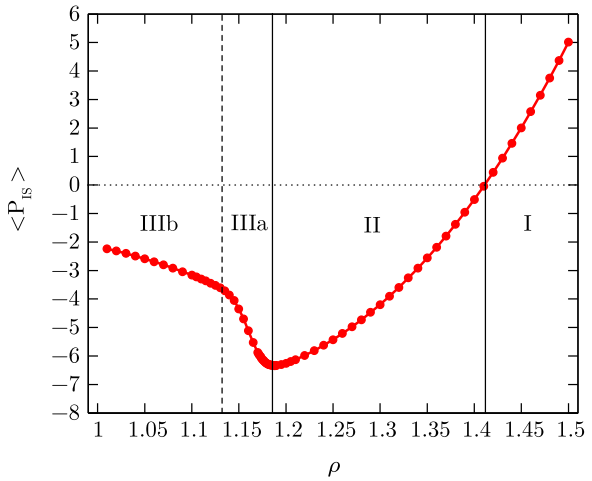

FIG. 3. Equation of state of the energy landscape for the (7,6) potential ($N = 500$). In region I, inherent structures are under compression ($P_{IS} > 0$); in region II, they are under isotropic tension and spatially homogeneous; in region IIIa, the parent liquid samples both homogeneous and fractured inherent structures; in region IIIb, all inherent structures are fractured. See text for further details.

tension. The features discussed so far have been reported in previous characterizations of this phenomenology.[14,15,29,35] The new feature, discussed below, is the subdivision of the third region below the Sastry density, denoted by a vertical dashed line.

The equation of state below ρ_S is now subdivided into two regions: the cross-over region IIIa and the fractured region IIIb. Previous descriptions[14] attached a singular significance to ρ_S, describing it as the density where the inherent structures can no longer both sustain isotropic tension and satisfy spatial homogeneity. Accordingly, all inherent structures produced below ρ_S were presumed to be fractured. However, this is not the case in this system. Rather, our observations are more consistent with ρ_S indicating the *onset* of fracture. We first describe this scenario qualitatively.

Reducing the density to just below ρ_S results in only a small fraction of the inherent structures fracturing. The majority remain homogenous and experience a larger isotropic tension than the inherent structures generated at larger density. The minimum in the equation of state at ρ_S is the result of a relatively small number of fractured inherent structures at much lower tension raising the average pressure. As the density is reduced further below ρ_S, the fraction of fractured structures increases, and the resulting equation of state exhibits lower tension. The range of densities where both fractured and homogenous inherent structures are sampled delineates the cross-over region. Once the density is reduced to roughly 1.13, only fractured structures are observed. Such a description arises by examining the distributions of inherent structure pressures and potential energies, as we explain below.

If all the inherent structures below ρ_S are fractured, one would expect the distribution of pressures to be unimodal and centered about its mean value, provided by the equation of state. Turning to the distributions presented in Fig. 4, we indeed see a unimodal distribution of inherent structure energies and pressures at ρ_S. However, as the density is reduced to just below ρ_S, a tail begins to develop on the low-tension side of the distribution. A modest decrease in density results in the distribution becoming bimodal due

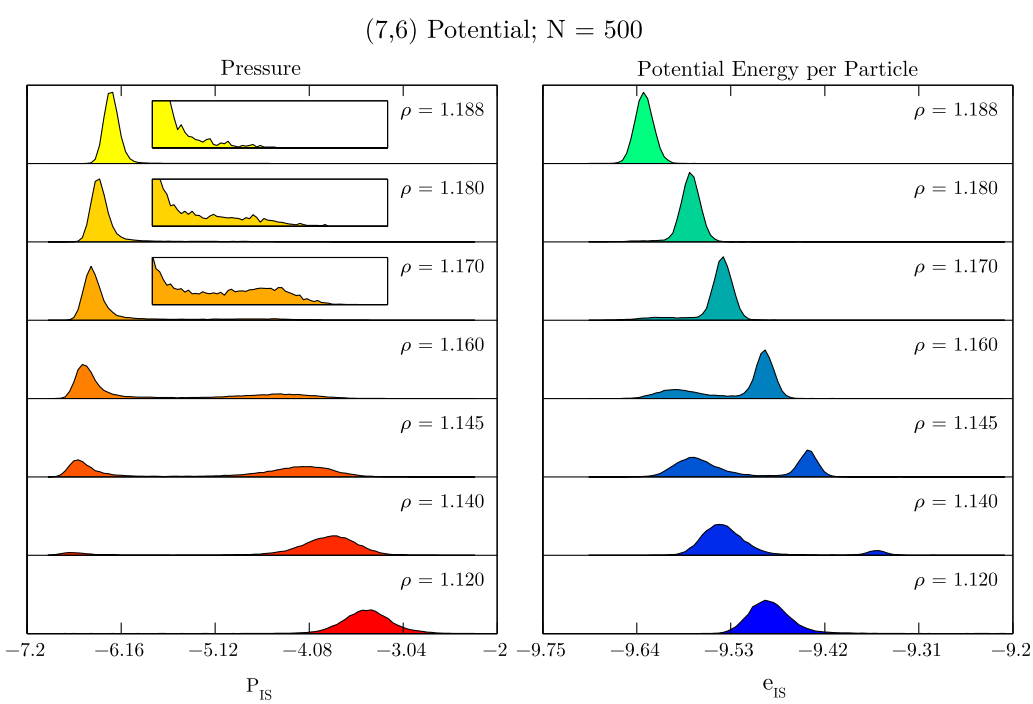

FIG. 4. Development of the distributions of the inherent structure pressure and potential energy per particle at and below ρ_S for the (7,6) potential ($N = 500$). Below ρ_S the distributions become bimodal due to a collection of homogeneous and fractured inherent structures being sampled by the parent liquid. At low enough density, the distributions become unimodal, and all inherent structures are fractured. The insets, demonstrating how the low-tension tail of inherent structure pressure distribution develops below ρ_S, range from $P_{IS} = -6.16$ to -3.04.

to a second peak emerging from the low-tension tail. Note that the high tension peak moves to even higher tensions as density is reduced. Inspection of the inherent structures reveals that configurations corresponding to the high tension portion are homogenous while those in the low tension portion are fractured. Further reduction in density results in the area under the high tension portion diminishing as the area under the low tension region grows. Thus, as the density is reduced further below ρ_S, a greater fraction of the inherent structures exhibit fracture. Once the density is reduced sufficiently below ρ_S, only a low tension peak remains, and all the inherent structures are broken.

We now turn to discussing the corresponding development of the distribution of inherent structure potential energy per particle, e_{IS} (right column of Fig. 4). The first observation of interest is that at fixed density within the cross-over region, broken inherent structures have lower (more negative) potential energies than homogeneous inherent structures. Similar to the behavior of the pressure distributions, slightly below ρ_S a tail develops on the low-energy side of the distribution, and this tail soon evolves into a second peak. This second peak augments as the original peak diminishes. Note that the behavior of the lower energy peak follows the evolution of the low tension peak.

Within the crossover region, the liquid samples two qualitatively different sets of basins of attraction: (1) basins with minima that correspond to homogeneous configurations and (2) basins that have minima with fractured (yet still mechanically stable) inherent structures. In either of these basins, the liquid itself is largely homogeneous, yet in the fractured basin, the path to the local energy minimum is accompanied by barrierless cavitation. Such fracture results in an inherent structure comprised of void-space and a dense particle region, the latter of which enables these packings to have much lower energy than their homogeneous counterparts.

Turning to the average inherent structure energy per particle as a function of density (Fig. 5), we see that the split behavior of the distributions of energy results in a loop. A local maximum occurs at roughly $\rho = 1.186$, a value essentially the same as the Sastry density. We proceed by observing that at sufficiently low density, $\langle e_{IS} \rangle$ is linear in density, and at sufficiently high density, it is quadratic. In other words, the curve can be parsed into two distinct branches: a homogeneous branch and a fractured branch. Fitting the data to these two functional forms and allowing for modest extrapolation yields a crossing point at about $\rho = 1.21$, a value greater than ρ_s. Above this intersection, the homogeneous branch has lower potential energy, and below, the fractured branch has lower potential energy. The cross-over region is a window where the liquid can "hop" between either branch, readily sampling both fractured and homogeneous basins of attraction. Such hopping results in a bimodal distribution of energy and pressure. As the density is reduced, the separation between branches increases, and the liquid samples basins corresponding to the lower energy fractured branch with increasing proportion. At low enough density, the liquid exclusively samples the fractured branch and the distribution returns to being unimodal.

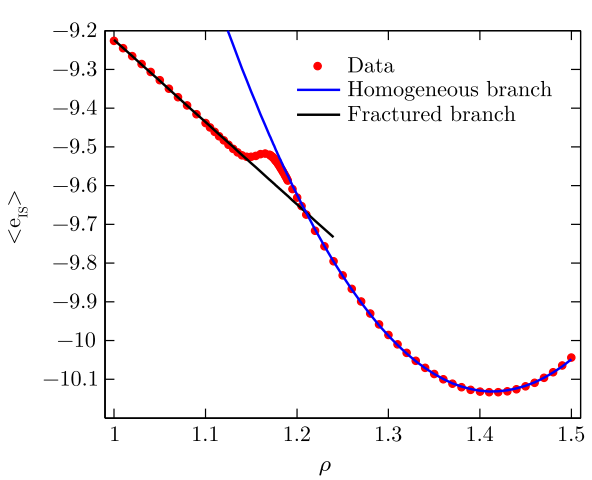

FIG. 5. Average inherent structure energy per particle for the (7,6) potential ($N = 500$). The curve is divided into distinct homogenous and fractured branches.

IV. SYSTEM SIZE EFFECTS

Here we show that the spinodal-like Sastry point and the accompanying bimodality of the pressure and potential energy arise as a result of the system's finite size. The evolution of the equation of state of the energy landscape with system size resembles previous observations of finite-sized rounding of the vapor/liquid transition in simulations. Such a development suggests that the behavior considered here may be a finite-size manifestation of an underlying athermal first-order phase transition.

A. Behavior of average properties

The presence of finite-size effects is illustrated through both the (7,6) and a (12,6) version of the generalized (n,6) Lennard-Jones potential. Inherent structures along the $T = 1.0$ isotherm were generated for system sizes ranging from 500 to 20 000 particles for the (7,6) version and 500 to 60 000 particles for the (12,6) version. For runs with 500 particles, 25 000 independent configurations at each density were used to generate inherent structures. For system sizes ranging from N = 1000 to 4000, 10 000 configurations were used; N = 8000 used 5000 configurations; N = 20 000 used 1500; N = 60 000 used 600 configurations.

From Figure 6, it is immediately clear that Sastry behavior is subject to finite size effects. We begin by considering the equation of states for the two versions of the potential considered here (first row in Fig. 6). At higher density, the curves exhibit very modest system size dependence. However, as one reduces density, these curves "peel-off" at different densities, with larger system sizes peeling off at higher density, resulting in a minimum that is now system-size dependent. In other words, the location of the Sastry point (both its density and the corresponding tension) is a function of system size. In addition, the region of the equation of state just below ρ_S becomes much steeper with increasing system size, suggesting

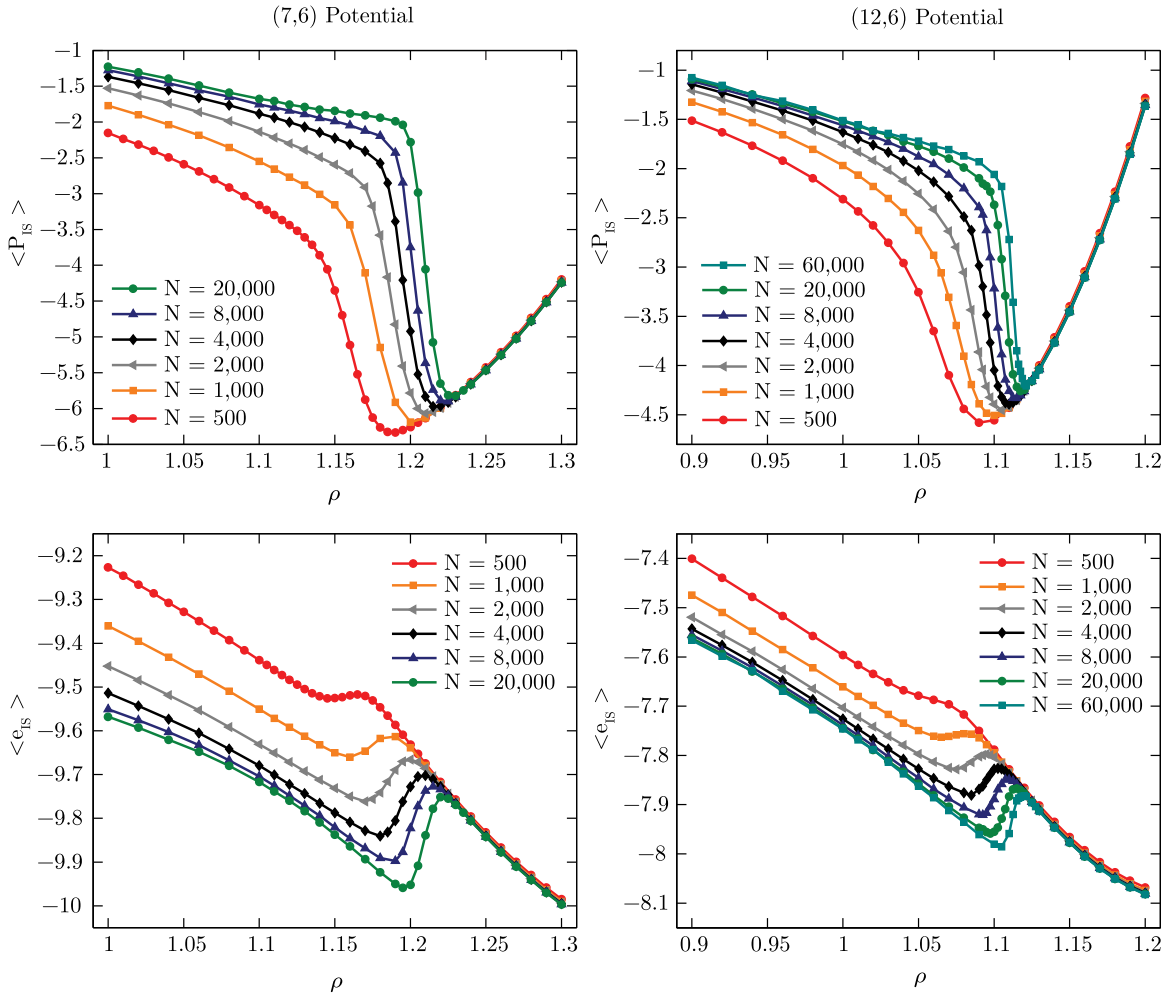

FIG. 6. System size effects for the (7,6) and (12,6) potentials in both the inherent structure equation of state and the average potential energy per particle.

a more abrupt transition from exclusively homogenous to exclusively fractured inherent structures. Within the range of densities shown here for the (12,6) variant, only the system sizes of 20 000 and 60 000 appear to converge to a large system-limit at lower density. For the (7,6) variant, system sizes of 8000 and 20 000 appear close to converging to the large-system limit at low density.

The finite-size effects observed here bear resemblance to the behavior of the equation of state of molecular liquids in NVT simulations. As the density of the liquid is reduced (below the range of densities considered here), it will ultimately undergo cavitation, and the equation of state will display a minimum. Such a minimum is often interpreted as a spinodal. However, it is in fact a consequence of finite-size rounding of the first-order vapor/liquid transition.[49] Likewise, this liquid "spinodal" point shifts to higher density with increasing system size,[50] and bimodality in the potential energy is observed in the neighborhood of the minimum.[51] We stress that the $T = 1.0$ equilibrated liquid isotherm remains unchanged with system size for the range of densities considered here. It thus appears that the Sastry point is subject to similar finite-size rounding.

The average potential energy per particle (second row Fig. 6) also exhibits finite-size effects. Similar to the equation of state, at high enough density, there is little change with system size. Likewise, the position of the local maximum shifts to higher density with increasing system size, as the liquid begins to predominantly sample the fractured branch. In addition, the density difference between the local extrema diminishes, demonstrating the occurrence of a more abrupt transition. In addition, the separation in inherent structure energy between the two extrema widens with system size. It appears that while the function describing the homogeneous branch is nearly system size independent, it is largely the fractured branch that exhibits strong system size effects. Not only does the fractured branch shift to lower energy as system size increases, it also changes shape. As system size increases, what could pass for linear energy vs. density behavior at modest system sizes acquires progressively more pronounced negative curvature.

B. Behavior of distributions crossing the Sastry point

As discussed in Section III, examining the distributions of inherent structure pressures and energies resulted in the insight that the Sastry density is where the liquid begins to sample fractured basins of attraction. The behavior of the average quantities (pressure and energy) within the crossover region reflects the proportion of either the homogenous or the fractured branches that the liquid samples. Here, we discuss

how these distributions evolve with system size to yield the average behavior discussed above.

In Figures 7 and 8, for system sizes ranging from 500 to 20 000, we provide the distributions of pressure and energy for a range of densities crossing the Sastry density for the (7,6) and (12,6) versions of the potential. Since the Sastry density changes with system size, a different density range is presented for each system size. As expected, all peaks become sharper with increasing system size. Both the (7,6) and (12,6) variations begin to exhibit bimodality at higher density as the system size increases, consistent with the observation that ρ_S increases with system size. For both pressure and energy, the separation of the two peaks is more dramatic with increasing system size. Widening of the separation between the peaks is consistent with a more sudden increase in pressure below ρ_S as well as the widening in the energy difference between the local extrema in Fig. 6. In addition, the density range over which bimodality is observed shrinks with system size, consistent with the more abrupt transition observed in the average properties as the system size increases. The behavior of the distributions also suggests that the width of the crossover region diminishes with system size, a reflection of

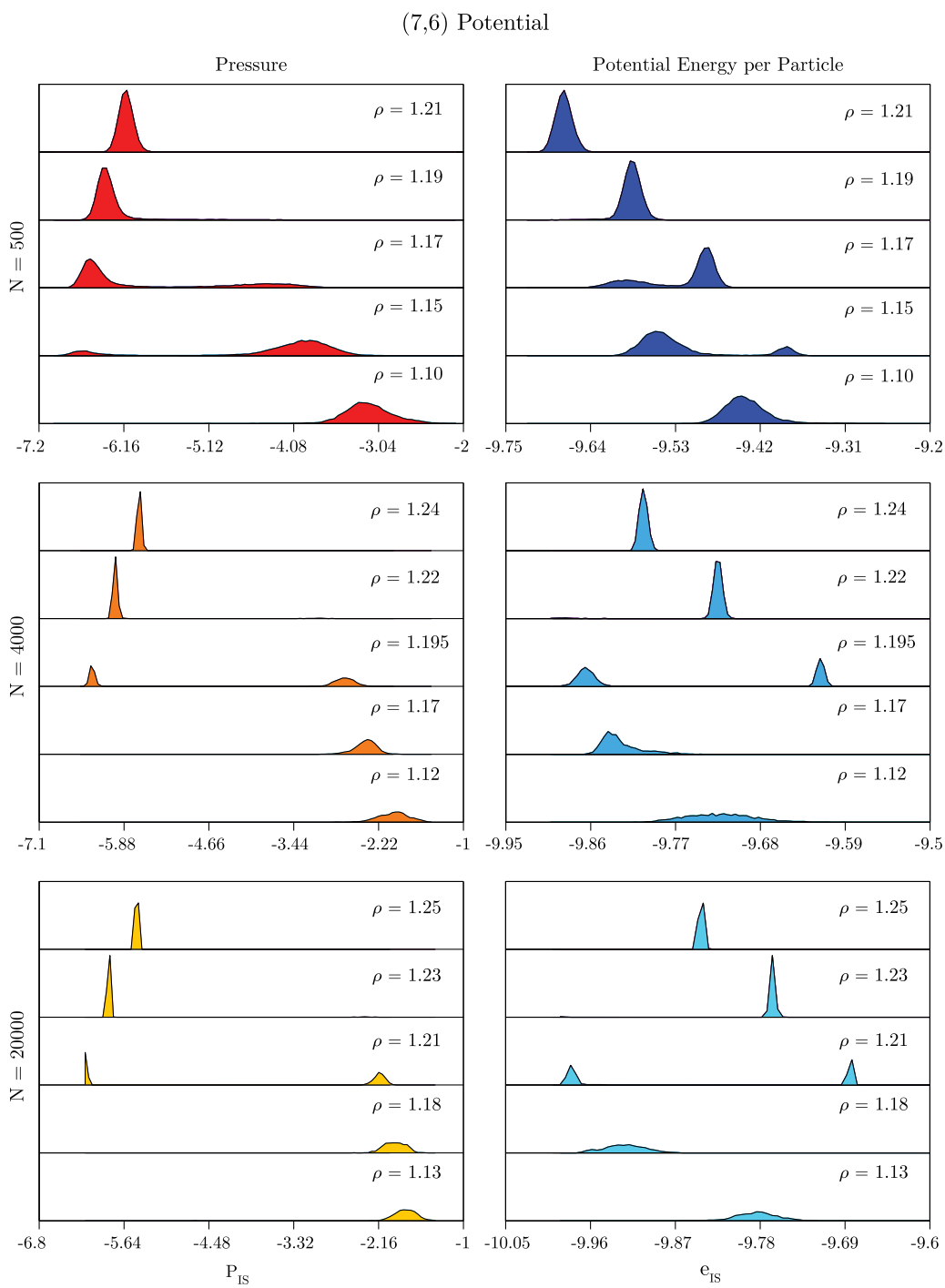

FIG. 7. Development of the distributions of the inherent structure pressure and potential energy per particle crossing ρ_S as a function of system size for the (7,6) potential.

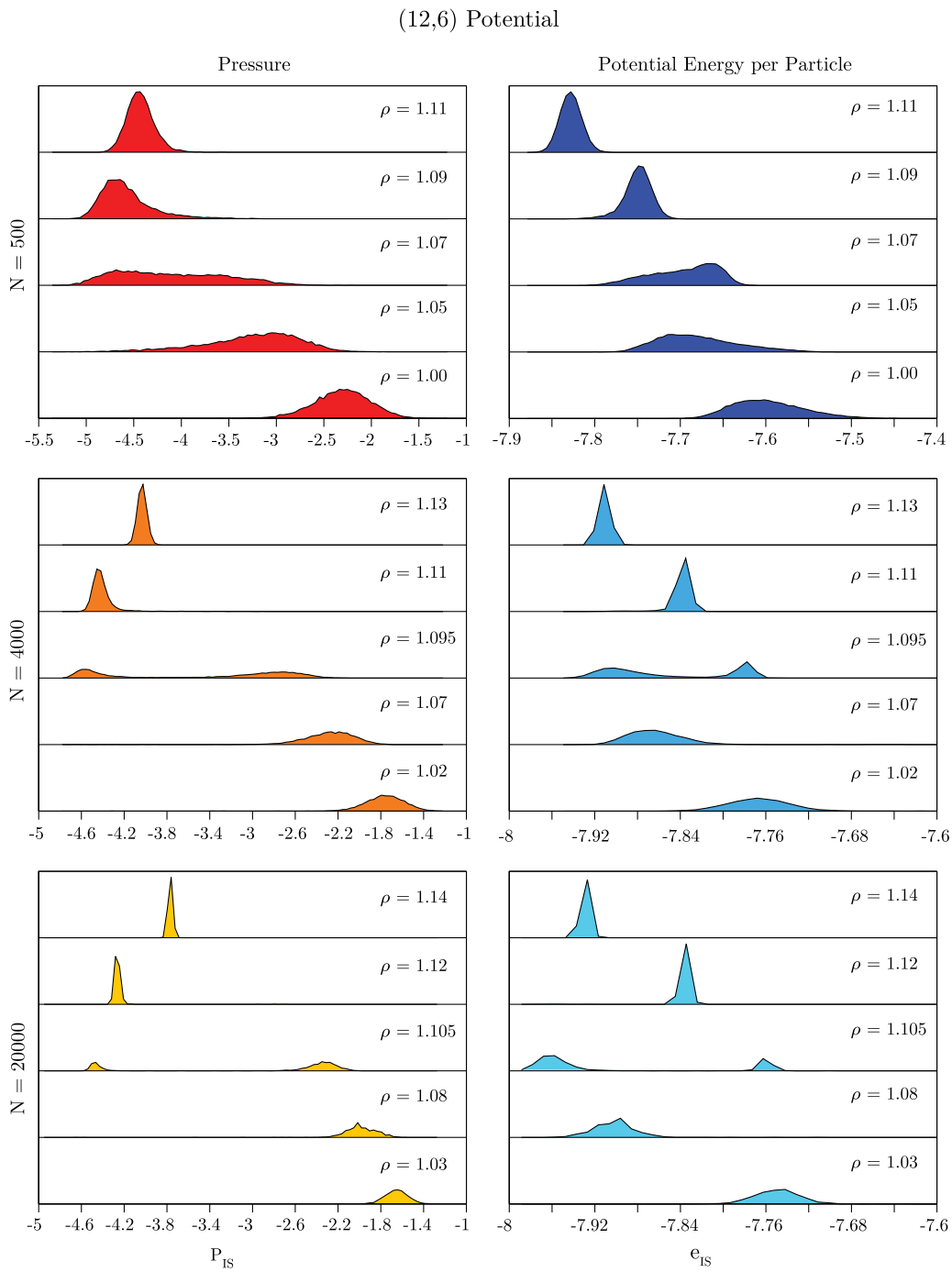

FIG. 8. Development of the distributions of the inherent structure pressure and potential energy per particle crossing ρ_S as a function of system size for the (12,6) potential.

the liquid transitioning more abruptly to exclusively mapping onto fractured inherent structures.

C. Void surface characterization

Instantaneous interface representations[37] of the void space provide a set of points that delineate the boundary between the void space and compact particle regions. If a particle was within a distance of 1 from any point on that boundary, it was counted as a surface atom. Figure 9 shows how the average number of surface atoms develops with density and system size in both the systems that we have considered. At sufficiently high density, the number of surface atoms is zero, as no fracture occurs at those points. At ρ_S for a given potential and system size, the curve departs from zero and increases monotonically with decreasing density. In the neighborhood below ρ_S, we observe a mixture of configurations with voids and with exactly zero surface atoms, again showing that bimodality in the pressure and potential energy is due to presence of both homogeneous and fractured inherent structures. In the averages presented here, the kink in the curves, most notable for the largest system size, marks the end of the cross-over region, and below that point, only fractured inherent structures are observed.

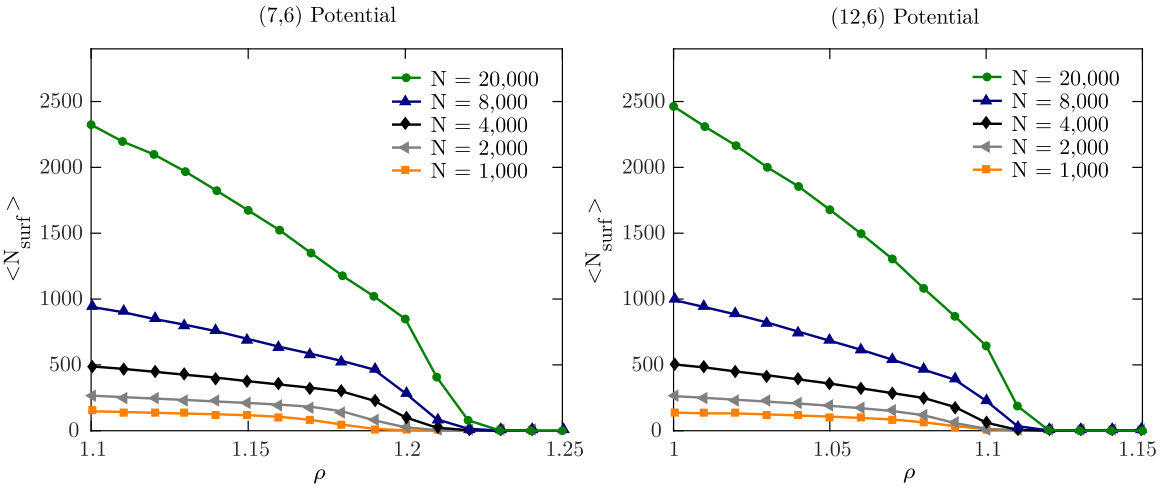

FIG. 9. Average number of surface atoms $\langle N_{\text{surf}}\rangle$, the number of particles at the interface between the void space and compact particle region, of inherent structures for the (7,6) and (12,6) potentials.

While the overall A:B composition is 80:20, we have found that the fraction of A particles at the surface is largely greater than 90%. Such an enrichment of A at the surface is preferable energetically, as placing a B at the surface sacrifices attractive AB pair interactions, the strongest in this mixture. It appears that concentration fluctuations in the liquid which result in regions that are enriched in component A create "weak spots"[29] that facilitate cavitation upon minimization. We expect that such "weak spots" should also serve as preferential sites for cavitation in the same binary system at finite temperatures.

D. Potential softening

Studying both the traditional (12,6) and the softer (7,6) version of the (n,6) potential allows us to comment on the effect of potential softening in the context of the Sastry phenomenology. The softer version of the potential exhibits bimodality at much smaller system size (see top rows of Fig. 7 vs. Fig. 8). For systems of 500 particles, the (7,6) variant shows bimodality, while the pressure and energy distributions of the (12,6) variant lack two distinct peaks. Rather, the distributions become smeared and asymmetric as density is reduced, owing to overlap in the distributions at small enough system size. The original studies of the Sastry phenomenon used the more common (12,6) variant (both single component and Kob-Andersen mixture) with 256 particles,[29,30] a system size below the threshold for observing bimodality in the (12,6) version. Thus, bimodality in the inherent structure properties, which only emerges either with potential softening or with larger system size, went unnoticed.

V. BEHAVIOR IN THE THERMODYNAMIC LIMIT

Given the strong finite-size effects discussed above, we now consider how Sastry behavior is likely to manifest itself for typical molecular liquids in the thermodynamic (infinite system size) limit. The first clue we turn to is the observation that the cross-over region shrinks as system size increases. In the distributions of pressure and energy, this trend presents itself in the narrower density window over which bimodality is observed. In the inherent structure equation of state, a narrower cross-over region results in the curve just below ρ_S becoming increasingly steep. For the average potential energy per particle, the density difference between the two local extrema shrinks with system size. If these trends were to persist, the limiting behavior at infinite system size would result in discontinuities in both the equation of state and potential energy. In such a scenario, the width of the density range constituting the cross-over region would be exactly zero.

Such behavior would be due to a sharp transition in the liquid. Above ρ_S, the liquid exclusively resides in basins with minima that correspond to homogeneous inherent structures. Below ρ_S, the liquid samples basins with minima that are fractured. To some extent the original interpretation of the Sastry point is preserved in such a scenario. The minimum in the inherent structure pressure equation of state is a sharp transition separating homogeneous and fractured inherent structures.

To estimate ρ_S in the thermodynamic limit, we first calculate the fraction of homogeneous inherent structures f_{homo}, using the fact that such packings will have zero surface atoms (see Sec. IV C). The f_{homo} versus density curve has an S-shape, and is well described by

$$f_{homo}(\rho) = \frac{1}{1 + \exp\left[-k\left(\rho - \rho_{1/2}\right)\right]}, \tag{4}$$

where k is a constant describing the steepness of the transition and $\rho_{1/2}$ is the density where sampling homogeneous and fractured inherent structures are equally probable (i.e., $f_{homo}\left(\rho_{1/2}\right) = 1/2$). Fitting the available data to Eq. (4) yields an estimate of $\rho_{1/2}$, which we consider as the nominal location of the transition in a finite system. For both versions of the potential, $\rho_{1/2}$ size dependence follows roughly a $1/N^{1/3}$ scaling law. We emphasize that such scaling is an empirical finding not associated with any theory. Approaching the

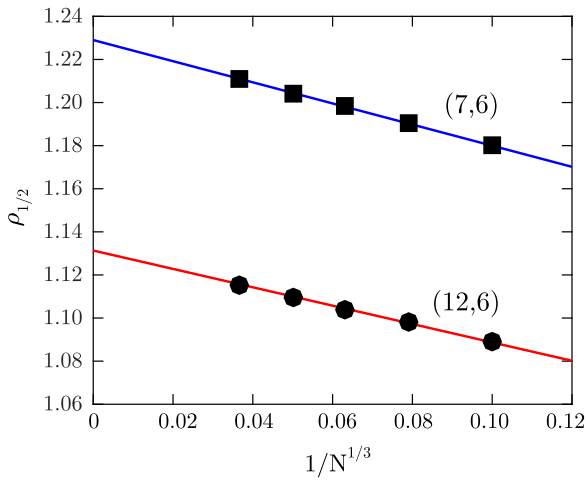

FIG. 10. Finite-size scaling of $\rho_{1/2}$, the density where homogeneous and fractured inherent structures are sampled in equal proportions by the parent liquid, for the (7,6) and (12,6) potentials. In the thermodynamic limit, $\rho_{1/2}$ and ρ_S will converge to a single value.

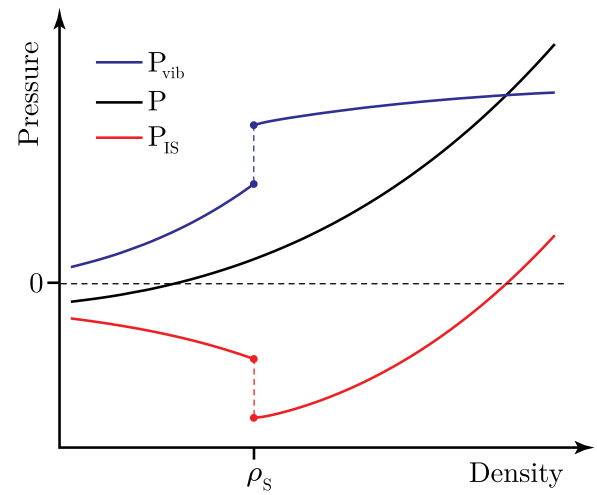

FIG. 11. A schematic liquid equation of state crossing the Sastry density along with its corresponding inherent structure and thermal contributions. If the inherent structure equation state is discontinuous at the Sastry density, continuity of the liquid's pressure requires that the thermal ("vibrational") contribution to the pressure undergo a compensating discontinuity.

thermodynamic limit, $\rho_{1/2}$ and ρ_S will converge to a single value. Figure 10 displays this scaling, and suggests that in the thermodynamic limit ρ_S for the (7,6) potential is 1.229 and for the (12,6) potential is 1.131.

The inherent structure formalism decomposes the partition function into contributions from the distinct inherent structures and the deviations from those minima that arise from thermal motion.[16] Such a decomposition allows the free energy and in turn all thermodynamic properties to be expressed as the sum of an inherent structure contribution and a thermal contribution,[14] often referred to as a "vibrational" contribution. In the context of the liquid's equation of state, one may express the pressure as

$$P = P_{IS} + P_{vib}, \tag{5}$$

where P_{vib} is the contribution that arises from thermal motion. We have suggested that P_{IS} exhibits a discontinuity at the Sastry point in the thermodynamic limit. However, P itself is continuous at ρ_S. Thus it must be that at the Sastry point, P_{vib} exhibits a discontinuous negative jump to precisely compensate for the discontinuous positive jump in P_{IS}. A schematic of the liquid equation of state along with its inherent structure and vibrational decomposition in the neighborhood of ρ_S is presented in Fig. 11.

We now turn to discussing the implications of these observations for a typical equilibrium phase diagram. In agreement with previous observations,[29,30] we see negligible effects of temperature on the location of ρ_S. The only exception that we have found is by sampling the $T = \infty$ fluid distribution, created by generating random configurations of particles at a given density, which upon minimization, exhibits a Sastry point at slightly higher density. This suggests that somewhere between typical fluid temperatures and infinite temperature, there is a modest increase in the Sastry density.

The modest temperature dependence of ρ_S suggests that there is a nearly vertical line in the temperature-density plane that separates the state points that map to homogeneous inherent structures and those that map to fractured inherent structures. In Fig. 12, we present a schematic of the temperature-density phase diagram for a typical, single component material where such a line has been included. Previous work suggests that the Sastry density is close to the zero temperature extension of the liquid spinodal,[30] placing the line well above the critical density. Its position with respect to the triple point density remains to be clarified. The portion penetrating the binodal, denoted by a dashed extension, is only applicable to metastable liquids that have resisted cavitation. In sum, Sastry behavior separates the phase diagram into two non-overlapping regimes: one that samples homogeneous basins of attraction and another that samples fractured basins.

Though our observations here are supported by a binary mixture (designed specifically to inhibit crystallization), we

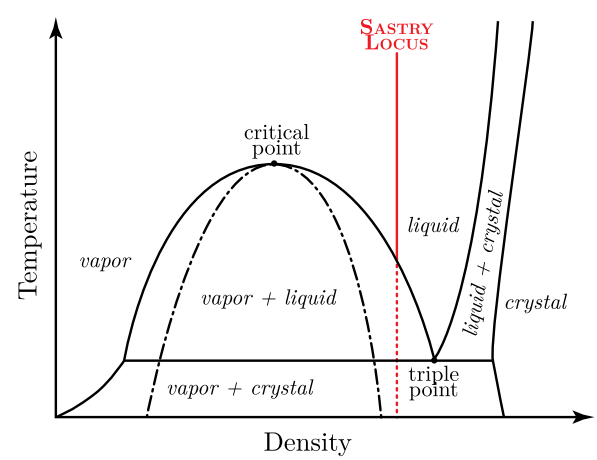

FIG. 12. The weak temperature dependence of the Sastry density suggests that a nearly vertical Sastry locus separates the phase diagram into two non-overlapping regions. Densities above ρ_S produce homogeneous inherent structures and densities below ρ_S result in fractured inherent structures. The precise location of this line with respect to the triple point requires future clarification.

have performed calculations with single component (7,6) and (12,6) generalized Lennard-Jones systems up to N = 4000, and we observe similar trends to those reported above. The strong attractions between components in the mixture considered in this work inhibit demixing. However, for mixtures more prone to component separation, the density of spontaneous demixing along an isotherm may preempt single-phase Sastry behavior. It may be that the two phase-separated portions of the liquid would have distinct Sastry points.

VI. ATHERMAL QUASISTATIC EXPANSION

We now turn to considering similar physics of cavitation in inherent structures through a different procedure: athermal quasistatic expansion. In the procedure we adopt here, the initial inherent structure configurations are generated through energy minimization of configurations from a $T = 1.0$ liquid at a given density above ρ_S. Following the initial minimization, the density of the inherent structure system is reduced by scaling the particle sizes (i.e., σ_{ij} where $i, j = AA, BB, AB$) down by 0.01%, followed again by energy minimization. Sequentially reducing density and minimizing constitute athermal quasistatic expansion. Similar protocols have been applied in numerous studies of plasticity in amorphous solids dating back to the early 1980s.[52–54] The procedure considered here is identical to that employed in a number of studies on the jamming scenario in granular media.[25,26,55]

Such a procedure corresponds physically to limiting regimes of two governing relaxation time scales, thermal relaxation τ_T, and mechanical relaxation τ_M, with respect to the expansion rate $\dot{\rho}$.[54,56] Temperatures must be sufficiently low that $\dot{\rho}/\rho \gg 1/\tau_T$, meaning thermal relaxation is entirely absent. On the other hand, the expansion rate must be low enough such that $\dot{\rho}/\rho \ll 1/\tau_M$, so that mechanical relaxation can proceed fully in response to a given density perturbation.

Athermal expansion represents a fundamentally different way of exploring a system's density-dependent energy landscape than minimizing liquid configurations at different densities. Results presented above characterized the basins of attraction most readily sampled by an equilibrium liquid. The series of density perturbations and minimizations presented in this section explores how a particular minimum evolves with density. We limit this section to discussing results for the (7,6) version of the potential, though similar results are obtained for the (12,6) version.

The presentation of the results in this section is similar to that above in the sense that we will mostly consider "ensemble" averages. "Ensemble" here is used rather loosely, as the averaging is over many expansions that start from the same density ρ_0. Specifically, the average inherent structure property M_{IS} at a given density ρ is calculated through an average over many expansion runs,

$$\langle M_{IS}(\rho)\rangle = \frac{1}{N_r}\sum_{i=1}^{N_r} M_i(\rho), \tag{6}$$

where N_r is the number of runs starting from the same density ρ_0. $\langle P_{IS}(\rho_0)\rangle$ will accordingly coincide with a point on the traditional inherent structure equation of state.

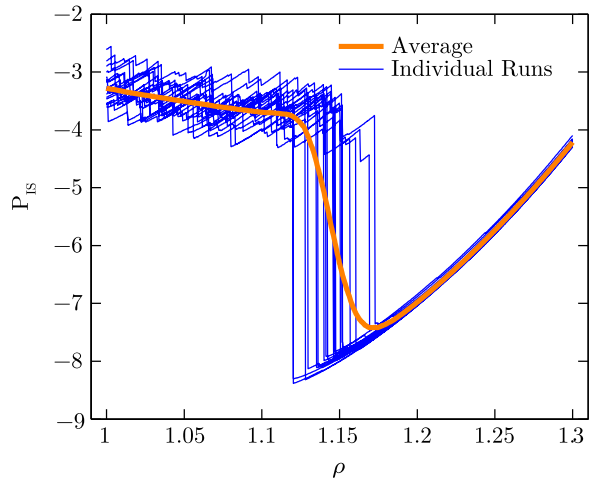

FIG. 13. The inherent structure pressure for 20 individual athermal quasistatic expansions and the average of 5800 runs for a system of 1000 particles interacting via the (7,6) potential.

An example of such averaging over 5800 expansion runs is presented in Fig. 13 along with 20 representative runs, all originating at $\rho_0 = 1.30$ for a system size of 1000 particles. The general trend is that all trajectories experience progressively greater isotropic tension upon expansion until reaching a density where roughly 50% of the tension is suddenly relieved as the system undergoes catastrophic failure due to cavitation. This sudden release of tension is accompanied by a dramatic decrease in potential energy. Following failure, further expansion is followed by a saw-tooth pattern in both the pressure and potential energy. The linear portions of this pattern correspond to an elastic response, and the jumps correspond to plastic events, similar to what has previously been observed in athermal shear flow.[56,57]

Numerous individual trajectories are averaged together to produce a smooth equation of state. This curve exhibits a minimum at a density which we will call ρ_A (for "athermal") in order to distinguish results of the two procedures. Similar to the results presented in Section II, the minimum at ρ_A is due to a small fraction of trajectories fracturing and again signals the *onset* of fracture. Most trajectories exhibit fracture between $\rho_A = 1.11$ and 1.17, a range that delineates the equivalent of the cross-over region within this procedure. At low density, the equation of state (unlike the individual trajectories) is smooth, suggesting that while individual trajectories will experience a series of elastic expansions separated by plastic events, they still oscillate about a characteristic density-dependent stress.

The existence of a cross-over region here again appears to be a symptom of finite system sizes. In Fig. 14 we present equation of state and trajectory averaged inherent structure energies as a function of system size. All initial inherent structures are generated from a $T = 1.0$ liquid at $\rho = 1.30$. As before, the curves are system-size independent at sufficiently high density. The equation of state exhibits a minimum at larger density with increasing system size. Likewise, $\langle e_{IS}\rangle$ exhibits a local maximum at larger densities for larger system sizes, and the low-density branches move to lower potential

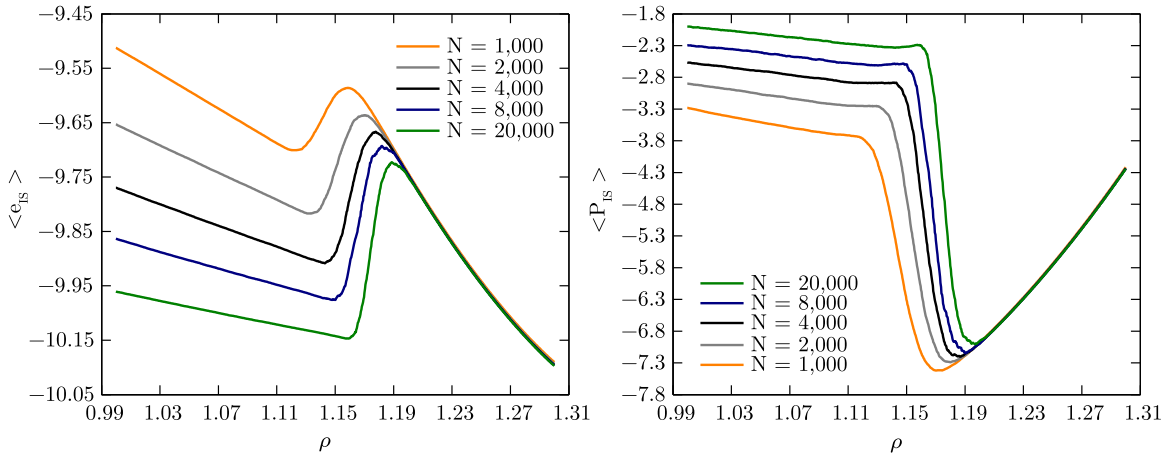

FIG. 14. System size effects in athermal quasistatic expansion for systems interacting via the (7,6) potential.

energy. Here too the cross-over region shrinks with system size, seemingly approaching a sharp discontinuity in the thermodynamic limit.

With these similarities noted, several interesting distinctions arise between the results of athermal expansion and the traditional equation of state of an energy landscape (Fig. 6). For the same system size, $\rho_S > \rho_A$ and $|P_S| < |P_A|$, meaning the limits of expansion are extended (lower density, higher isotropic tension) through athermal expansion. In fact for the whole procedure this equation of state is always below that of the traditional method. Surprisingly, until one is close to fracture, there is little difference between $\langle e_{IS} \rangle$ for the two procedures. At sufficiently low density, where all configurations are fractured, the athermal expansion procedure results in both lower energy and higher tension with respect to the traditional method. Recall that the potential energy

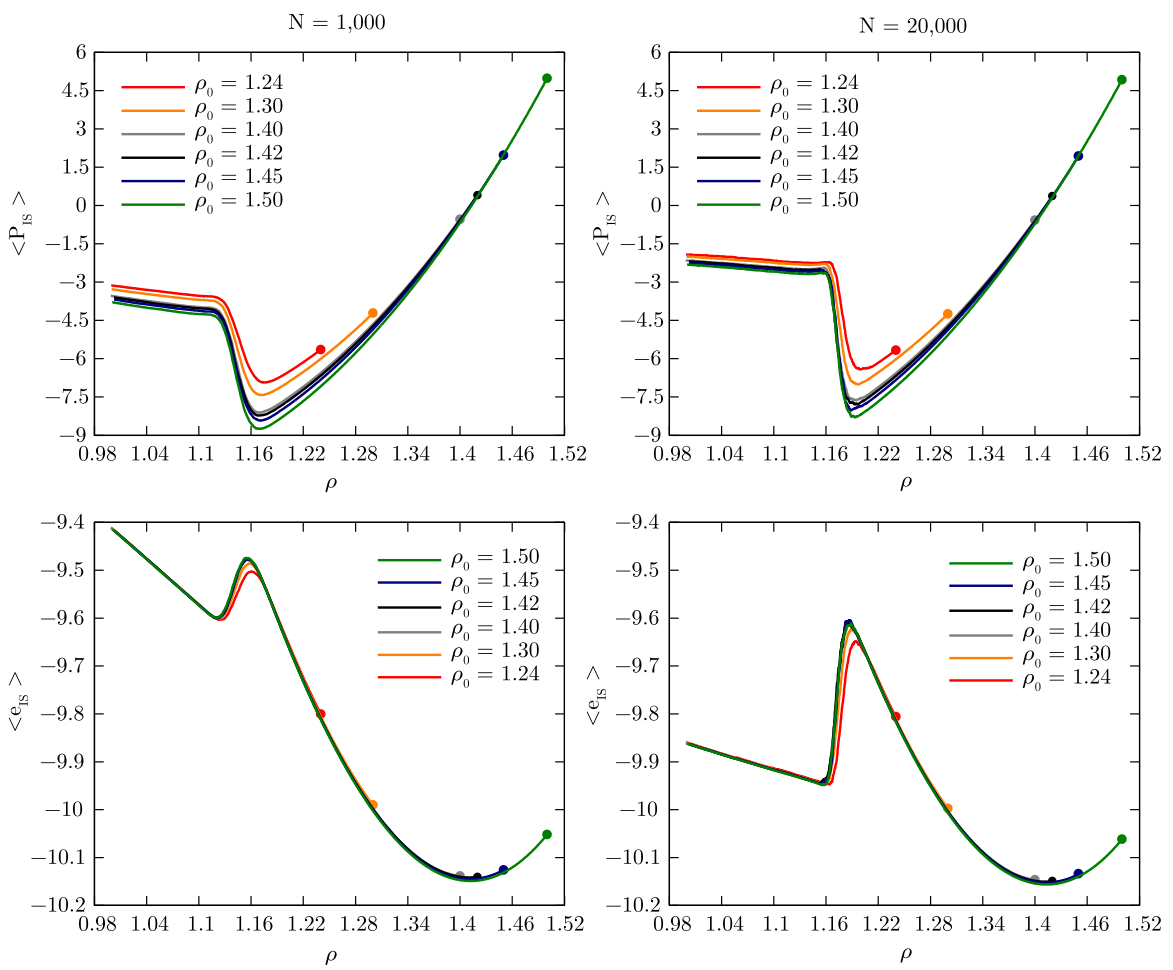

FIG. 15. Effect of the initial density of athermal quasistatic expansion on the average inherent structure properties for two system sizes interacting via the (7,6) potential.

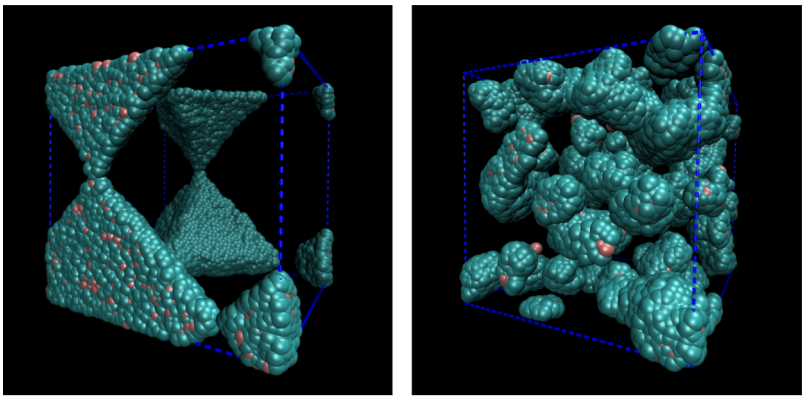

FIG. 16. Two configurations that correspond to minima on the same potential energy landscape [(7,6) potential; $N = 20\,000$; $\rho = 0.20$]. The configuration on the left is produced through athermal quasistatic expansion from $\rho_0 = 1.30$; the one on the right is an inherent structure of a supercritical fluid.

landscape is fixed for a given density. It would appear then that higher tension minima exist at these lower densities but are not sampled as frequently or at all by the equilibrium liquid.

We now consider how the starting density affects the mechanical limits of an amorphous solid. Again, all starting configurations are initially generated from a T = 1.0 equilibrium liquid. Here, we present results for system sizes 1000 and 20 000 (Fig. 15). ρ_A is fairly insensitive to starting density, though it appears that the largest starting density has a slightly lower ρ_A. However, larger starting densities result in larger maximum tension, meaning the high density glasses produced in this manner are stronger than the low density glasses. It is interesting to note that even though all starting densities share a common ρ_A, the higher-density glasses must undergo far greater strain before fracture occurs. Part of this fact is simply attributable to the fact that the material obtained from higher initial densities starts under compression, so an initial portion of the strain is dedicated to bringing the system under tension. Surprisingly, the potential energies appear only to deviate in the crossover region with the remaining portions being almost identical. Apparently, different starting densities follow paths that are on average identical in potential energy, yet the packing arrangements inherent to those paths have different stresses.

Unlike equilibrium systems, materials out of equilibrium, such as glasses, will have properties that depend on their processing histories. Our results suggest a route to producing a stronger glass. Producing a glass under high compression and then slowly allowing it to relax to ambient pressures should result in a material with a larger ultimate yield stress than a glass similarly quenched at ambient pressure. It is also likely that the cooling rate employed in producing the high compression glass, something we have not explored here, would be an important design input for such a procedure.

The starkest difference we have observed so far between minimizing from an equilibrium fluid and athermal expansion is in the morphologies of inherent structures at low density. The configuration on the left in Figure 16 is a system of 20 000 particles at $\rho = 0.20$ that has undergone an athermal expansion run from $\rho_0 = 1.30$. The void that forms upon cavitation has simply grown upon further expansion to accommodate the additional volume. On the right is a configuration minimized at $\rho = 0.20$ and $T = 2.0$, which is slightly above the critical temperature. Here we observe a number of separate clumps of particles. Both of these configurations are minima on the same potential energy landscape, and it is temperature and processing history that distinguish the pathways to these minima.

VII. CONCLUDING REMARKS

In a sense, the present work has demonstrated how cavitation in the liquid phase is imprinted in the underlying potential energy landscape. The cavitation that inevitably appears in a molecular liquid upon decompression is preempted by a sudden shift in the type of basin sampled at the Sastry density. Above ρ_S all inherent structures are homogeneous, and below ρ_S all are fractured. The signature of this transition is likely a discontinuity in the equation of the state of the energy landscape. However, this athermal transition at ρ_S is subject to finite-size rounding, and the above description is only realizable in the thermodynamic limit. Like previous characterization of the vapor/liquid transition, the Sastry point appears spinodal-like at finite system sizes. Due to continuity in the liquid's pressure, a discontinuity in the behavior of the inherent structures also implies a perfectly compensating discontinuity in the thermal stabilization of the liquid.

If the Sastry locus intersects the vapor/liquid binodal (as illustrated in Fig. 12), cavitation in liquids produced through isochoric cooling will follow qualitatively different pathways on the potential energy landscape above and below ρ_S. Liquids below the Sastry density can cavitate simply by the descending to lower energy regions of the basin of attraction they already occupy. Above ρ_S, a liquid would need to transition to a different basin of attraction in order to cavitate.

We have also demonstrated that Sastry behavior is not just a feature of the landscape sampled by an equilibrium liquid but is in fact also relevant to the physics of non-equilibrium stretched glasses. In this case, we studied the behavior of packings subject to athermal quasistatic expansion. Averaging over many expansion trajectories yields an equation of state that is qualitatively similar to that produced from sampling the inherent structures along an equilibrium liquid isotherm.

Likewise, this equation of state is subject to finite size effects and displays analogous behavior to finite-size rounding. The limiting tension increases with the starting density of an expansion run, suggesting that glasses produced under high compression will have a larger ultimate yield stress. The athermal characterization in this study should apply to finite temperature glasses that are expanded slowly at sufficiently low temperatures, and at least one study[58] to date has observed similar behavior in the equation of state of a (12,6) Kob-Andersen system subject to expansion at low temperatures.

The picture we have developed here is expected to be general for simple liquids and their mixtures. Liquids with internal directional constraints such as liquid crystals or network forming liquids such as water may prove to provide richer phenomenology in the context of Sastry behavior. Characterizing Sastry behavior in metallic systems described by embedded-atom method[59] potentials would also be a fruitful extension of this work, and may shed light on existing studies of cavitation in metallic glasses at various applied tensile strains.[60] While we have observed minimal temperature effects in the present work, it is expected that probing the inherent structures above and below a λ-transition, such as the sudden viscosity change upon heating in liquid sulfur,[61,62] would yield a rich variety of mechanical behavior. In addition, it may be interesting to see how this behavior emerges for systems with metastable vapor/liquid transitions such as models of C_{60}.[3] We have suggested that for the liquid pressure (as well as other thermodynamic properties) to remain continuous across the Sastry density, there must be an abrupt change in the thermal or "vibrational" contributions to the pressure. This claim is simply based on accounting, and identifying what this abrupt change physically corresponds to would certainly enrich our understanding of the liquid state. A concrete calculation will likely require numerical evaluation of the intrabasin canonical partition functions for representative sets of inherent structures produced at densities that tightly bracket the Sastry density.

ACKNOWLEDGMENTS

Y.E.A. is grateful to Zane Shi for helpful discussions and Nyssa Emerson for figure preparation assistance. P.G.D. gratefully acknowledges the support of the National Science Foundation (Grant No. CHE-1213343).

[1] J. D. Weeks, D. Chandler, and H. C. Andersen, J. Chem. Phys. **54**, 5237 (1971).
[2] H. C. Andersen, D. Chandler, and J. D. Weeks, Adv. Chem. Phys. **34**, 105 (1976).
[3] M. H. J. Hagen *et al.*, Nature **365**, 425 (1993).
[4] M. H. J. Hagen and D. Frenkel, J. Chem. Phys. **101**, 4093 (1994).
[5] C. F. Tejero *et al.*, Phys. Rev. Lett. **73**, 752 (1994).
[6] P. R. ten Wolde and D. Frenkel, Science **277**, 1975 (1997).
[7] D. Levesque and L. Verlet, Phys. Rev. A **2**, 2514 (1970).
[8] J. Kushick and B. J. Berne, J. Chem. Phys. **59**, 3732 (1973).
[9] L. L. Lee and D. Levesque, Mol. Phys. **26**, 1351 (1973).
[10] S. D. Bembenek and G. Szamel, J. Phys. Chem. B **104**, 10647 (2000).
[11] L. Berthier and G. Tarjus, Phys. Rev. Lett. **103**, 170601 (2009).
[12] L. Berthier and G. Tarjus, J. Chem. Phys. **134**, 214503 (2011).
[13] S. Toxvaerd, Condens. Matter Phys. **18**, 13002 (2015).
[14] P. G. Debenedetti *et al.*, J. Phys. Chem. B **103**, 7390 (1999).
[15] C. J. Roberts, P. G. Debenedetti, and F. H. Stillinger, J. Phys. Chem. B **103**, 10258 (1999).
[16] F. H. Stillinger and T. A. Weber, Phys. Rev. A **25**, 978 (1982).
[17] F. H. Stillinger and T. A. Weber, Science **225**, 983 (1984).
[18] F. H. Stillinger, Science **267**, 1935 (1995).
[19] S. Sastry, P. G. Debenedetti, and F. H. Stillinger, Nature **393**, 554 (1998).
[20] P. G. Debenedetti and F. H. Stillinger, Nature **410**, 259 (2001).
[21] A. Heuer, J. Phys.: Condens. Matter **20**, 373101 (2008).
[22] F. H. Stillinger and P. G. Debenedetti, Annu. Rev. Condens. Matter Phys. **4**, 263 (2013).
[23] A. J. Liu and S. R. Nagel, Nature **396**, 21 (1998).
[24] C. S. O'Hern *et al.*, Phys. Rev. Lett. **88**, 075507 (2002).
[25] C. S. O'Hern *et al.*, Phys. Rev. E **68**, 011306 (2003).
[26] A. J. Liu and S. R. Nagel, Annu. Rev. Condens. Matter Phys. **1**, 347 (2010).
[27] C. P. Goodrich, A. J. Liu, and S. R. Nagel, Phys. Rev. Lett. **109**, 095704 (2012).
[28] D. S. Corti *et al.*, Phys. Rev. E **55**, 5522 (1997).
[29] S. Sastry, P. G. Debenedetti, and F. H. Stillinger, Phys. Rev. E **56**, 5533 (1997).
[30] S. Sastry, Phys. Rev. Lett. **85**, 590 (2000).
[31] R. A. LaViolette, Phys. Rev. B **40**, 9952 (1989).
[32] J. Hernandez-Rojas and D. J. Wales, Phys. Rev. B **68**, 144202 (2003).
[33] E. La Nave *et al.*, J. Chem. Phys. **120**, 6128 (2004).
[34] M. Utz, P. G. Debenedetti, and F. H. Stillinger, J. Chem. Phys. **114**, 10049 (2001).
[35] V. K. Shen, P. G. Debenedetti, and F. H. Stillinger, J. Phys. Chem. B **106**, 10447 (2002).
[36] R. A. La Violette, J. L. Budzien, and F. H. Stillinger, J. Chem. Phys. **112**, 8072 (2000).
[37] A. P. Willard and D. Chandler, J. Phys. Chem. B **114**, 1954 (2010).
[38] Z. J. Wang, C. Valeriani, and D. Frenkel, J. Phys. Chem. B **113**, 3776 (2009).
[39] F. H. Stillinger, P. G. Debenedetti, and T. M. Truskett, J. Phys. Chem. B **105**, 11809 (2001).
[40] S. S. Ashwin, G. I. Menon, and S. Sastry, Europhys. Lett. **75**, 922 (2006).
[41] Z. Shi *et al.*, J. Chem. Phys. **135**, 084513 (2011).
[42] W. Kob and H. C. Andersen, Phys. Rev. E **51**, 4626 (1995).
[43] T. A. Weber and F. H. Stillinger, Phys. Rev. B **31**, 1954 (1985).
[44] T. A. Weber and F. H. Stillinger, Phys. Rev. B **32**, 5402 (1985).
[45] S. Plimpton, J. Comput. Phys. **117**, 1 (1995).
[46] W. G. Hoover, Phys. Rev. A **31**, 1695 (1985).
[47] E. Polak and G. Ribiere, Rev. Fr. D Inf. De Recherche Operationnelle **3**, 35 (1969).
[48] W. Humphrey, A. Dalke, and K. Schulten, J. Mol. Graphics Modell. **14**, 33 (1996).
[49] L. G. MacDowell *et al.*, J. Chem. Phys. **120**, 5293 (2004).
[50] K. Binder *et al.*, Am. J. Phys. **80**, 1099 (2012).
[51] M. Schrader, P. Virnau, and K. Binder, Phys. Rev. E **79**, 061104 (2009).
[52] K. Maeda and S. Takeuchi, Philos. Mag. A **44**, 643 (1981).
[53] F. Leonforte *et al.*, Phys. Rev. B **72**, 224206 (2005).
[54] M. L. Falk and C. E. Maloney, Eur. Phys. J. B **75**, 405 (2010).
[55] P. Chaudhuri, L. Berthier, and S. Sastry, Phys. Rev. Lett. **104**, 165701 (2010).
[56] C. E. Maloney and A. Lemaitre, Phys. Rev. E **74**, 016118 (2006).
[57] C. Maloney and A. Lemaitre, Phys. Rev. Lett. **93**, 016001 (2004).
[58] P. Chaudhuri and J. Horbach, e-print arXiv:1509.03158 (2015).
[59] M. S. Daw and M. I. Baskes, Phys. Rev. B **29**, 6443 (1984).
[60] P. F. Guan *et al.*, Phys. Rev. Lett. **110**, 185502 (2013).
[61] B. Meyer, Chem. Rev. **76**, 367 (1976).
[62] T. Scopigno *et al.*, Phys. Rev. Lett. **99**, 025701 (2007).